Vol. 3, Iss. 2 (2026) 81-97, DOI: 10.61552/JMES.2026.02.004

Journal of Management and Engineering Sciences

www.jmes.aspur.rs

A High-Fidelity Simulink Model for Next-Generation EV Charging Infrastructure

Asif Eakball Emon[a,*]

[a] *Department of Electrical & Electronic Engineering, Faculty of Engineering and Applied Sciences, Bangladesh University of Business & Technology (BUBT), Dhaka, Bangladesh.*

Keywords:

Electric Vehicle (EV) Charger
High-Fidelity Modeling
Pulse Width Modulation (PWM)
Closed-Loop Control
Battery Management System (BMS)
DC-DC Converter
LLC Resonant Converter
Fast Charging
Vehicle-to-Grid (V2G)
Multi-Domain Simulation
Constant Current-Constant Voltage (CC-CV) Charging
Dq-Frame Control

* Corresponding author:

Asif Eakball Emon
E-mail:
eakballasif@gmail.com

Received: 27.12.2025.
Revised: 01.03.2026.
Accepted: 04.03.2026.

A B S T R A C T

The global transition to electric mobility demands advanced charging infrastructure capable of delivering high efficiency, superior power quality, and intelligent battery management while maintaining grid stability and thermal safety. Despite substantial progress in individual charger subsystems, the literature reveals a persistent gap in integrated modeling frameworks that capture the complex interdependencies between power electronics, control systems, battery dynamics, and thermal behavior, limiting system-level performance optimization. This research addresses this gap through the development and validation of a comprehensive high-fidelity MATLAB/Simulink model of a 50 kW two-stage electric vehicle charging system, integrating a three-phase active rectifier with dq-frame current regulation, an LLC resonant converter with frequency-modulated CC-CV control, a second-order Thevenin battery model, and a Cauer-type thermal network. The simulation results demonstrate that the proposed system achieves 1.92% current total harmonic distortion, 0.99 power factor, 94.3% peak efficiency, and 36-minute 20-80% state-of-charge charging time, meeting or exceeding IEEE 519 requirements. Furthermore, the integrated analysis reveals previously underappreciated system interactions including nonlinear coupling between DC-link ripple and LLC soft-switching margin, efficiency trajectory dynamics during charging cycles, and electro-thermal coupling affecting transition timing. This work establishes a validated virtual prototyping platform supporting design iteration and performance prediction for next-generation EV charging infrastructure, with implications for advancing reliable and grid-friendly charging solutions essential to sustainable transportation ecosystems.

1. INTRODUCTION

The global transportation sector stands at the precipice of a paradigm shift as electric vehicles (EVs) emerge as the cornerstone of sustainable mobility strategies worldwide [1]. With transportation contributing approximately 23% of global greenhouse gas emissions, accelerated EV adoption has become imperative for meeting international climate commitments [2]. This electrification revolution, however, hinges critically upon the parallel development of robust, efficient, and intelligent charging infrastructure capable of supporting millions of vehicles while maintaining grid stability and delivering acceptable user experience [3]. Contemporary EV charging systems must navigate a complex landscape of requirements including high power density, exceptional efficiency across wide operating ranges, minimal grid impact through power quality compliance, bidirectional energy transfer capability, and intelligent battery management that preserves cell longevity [4].

The fundamental challenge in EV charger design resides in the inherent tension between conflicting performance objectives that must be simultaneously satisfied within a single system [5]. The two-stage architecture comprising an AC-DC rectification stage followed by an isolated DC-DC conversion stage introduces complex interdependencies that complicate optimal design [6]. Despite substantial research progress in individual charger subsystems, the literature reveals a persistent gap in integrated, high-fidelity modeling frameworks that capture complete system dynamics with sufficient accuracy for design validation and optimization [7]. Prior investigations exist in isolation rectifier studies employing idealized DC loads, converter analyses assuming perfect DC sources, and battery investigations utilizing simplified charger models leaving critical interactions such as DC-link ripple effects on LLC soft-switching and coupled electro-thermal behavior inadequately characterized [8].

This research addresses this gap through the development and validation of a comprehensive, high-fidelity MATLAB/Simulink model of a 50 kW two-stage EV charging system that integrates detailed power electronics, advanced closed-loop control, validated battery dynamics, and electro-thermal coupling within a unified simulation framework [9]. The proposed model uniquely combines a three-phase active rectifier with dq-frame current regulation, an LLC resonant converter with frequency-modulated CC-CV control, a second-order Thevenin battery model, and a Cauer-type thermal network [10]. The principal contribution lies in establishing a validated simulation platform that captures full system dynamics to support design iteration and performance prediction, demonstrating through comprehensive results that the proposed architecture achieves 94.3% peak efficiency, 1.92% current THD, and 36-minute 20-80% SOC charging time [11].

The remainder of this paper is organized as follows: Section 2 presents a comprehensive literature review. Section 3 details the system architecture and modeling methodology. Section 4 presents and analyzes simulation results across steady-state, transient, efficiency, charging profile, power quality, and thermal performance dimensions. Section 5 concludes with key findings and future research directions.

2. LITERATURE REVIEW

The global transition toward electrified transportation has precipitated an urgent need for advanced, reliable, and high-performance electric vehicle (EV) charging infrastructure, with recent systematic analyses revealing that transportation accounts for approximately 23% of energy-related CO_2 emissions globally and road vehicles contributing nearly three-quarters of this fraction [12]. This environmental imperative, coupled with the geometric progression of electric vehicle adoption exceeding 10 million units sold globally in 2022, has necessitated fundamental reconceptualization of charging architectures capable of supporting widespread electrification while maintaining grid stability and delivering acceptable user experience [13]. Contemporary charging infrastructure must navigate a multidimensional design space bounded by conflicting performance objectives: ultra-fast charging capabilities ranging from 150 kW to 350 kW for passenger vehicles, scalability to megawatt-level systems for heavy-duty commercial fleets, bidirectional energy transfer for vehicle-to-grid applications, intelligent battery management ensuring cell longevity, and

seamless integration with intermittent renewable energy sources [14]. These requirements have positioned power electronic converters and their associated control systems at the epicenter of next-generation charging infrastructure research, driving investigation into advanced topologies, wide bandgap semiconductor applications, and integrated design methodologies that transcend traditional disciplinary boundaries [15].

The architectural evolution of EV chargers has converged on the two-stage configuration comprising an AC-DC rectification stage followed by an isolated DC-DC conversion stage, a topology that has demonstrated superior performance characteristics for high-power applications exceeding 50 kW [16]. This architecture, while theoretically capable of meeting stringent performance targets, introduces complex interdependencies that fundamentally complicate optimal design and demand holistic analytical frameworks [17]. The front-end AC-DC converter, typically implemented as a three-phase active rectifier with power factor correction, serves as the critical interface between the AC grid and the DC charging system, with control methodologies undergoing substantial evolution from conventional voltage-oriented control to sophisticated approaches including model predictive control, sliding mode control, and artificial intelligence-augmented strategies. Comparative analyses demonstrate that advanced control implementations achieve total harmonic distortion values consistently below 5% as mandated by IEEE 519 standards, with state-of-the-art systems reporting THD as low as 1.12% under nominal operating conditions [18]. The dq-frame current regulation approach, employing Park transformation for independent active and reactive power control, has emerged as the predominant methodology due to its favorable steady-state and dynamic characteristics, enabling simultaneous regulation of DC-link voltage and power factor with exceptional precision [19].

The isolated DC-DC converter has attracted considerable research attention, with the LLC resonant converter emerging as the preferred topology for high-power EV charging applications due to three inherent advantages: zero-voltage switching for primary-side switches across wide load ranges, zero-current switching for secondary-side rectifiers, and galvanic isolation capabilities essential for safety compliance [20]. Comprehensive reviews have systematically analyzed modulation strategies including pulse frequency modulation, phase-shift modulation, and hybrid approaches, establishing their respective advantages for bidirectional operation in V2X mode while demonstrating that the resonant tank design, characterized by the inductance ratio and quality factor, fundamentally determines converter performance with optimization studies revealing that inductance values between three and seven achieve optimal trade-offs between gain range and efficiency [21]. Beyond conventional silicon-based implementations, the integration of wide bandgap semiconductors, specifically silicon carbide and gallium nitride, represents a transformative trajectory in EV charger development, with comparative studies demonstrating that SiC MOSFETs enable switching frequencies exceeding 100 kHz while maintaining efficiencies above 98%, facilitating substantial reductions in passive component volumes and corresponding increases in power density [22]. The superior thermal conductivity of wide bandgap materials additionally enables operation at elevated junction temperatures reaching 200 degrees Celsius, simplifying thermal management requirements and enhancing reliability, while multilevel converter topologies including neutral-point-clamped and flying capacitor configurations have demonstrated particular promise for high-voltage EV charging applications by offering reduced device voltage stress and improved harmonic performance compared to conventional two-level implementations [23].

Accurate battery characterization constitutes a foundational requirement for optimal charging control, as state-of-charge and state-of-health determination fundamentally influences charging profile optimization and battery longevity [24]. Contemporary literature categorizes SOC estimation methodologies into four primary approaches with varying accuracy-complexity trade-offs, beginning with electrochemical models that offer the highest fidelity through physics-based representation of lithium-ion transport and intercalation kinetics while imposing computational demands prohibitive for real-time implementation in embedded systems, though recent advances in

reduced-order electrochemical modeling have partially addressed this limitation by achieving acceptable accuracy with seventy percent reduction in computational requirements. Equivalent circuit models, particularly the second-order Thevenin configuration, have gained widespread acceptance for their balanced complexity and accuracy in capturing battery dynamics including polarization effects and transient responses, enabling accurate terminal voltage prediction across diverse operating conditions through representation of charge transfer and diffusion phenomena via RC network dynamics with time constants spanning milliseconds to minutes [25]. Parameter identification methodologies for equivalent circuit models have advanced substantially, with online estimation techniques employing recursive least squares and extended Kalman filters demonstrating robust performance under dynamic loading conditions encountered during real-world driving and charging scenarios [26]. Data-driven approaches leveraging artificial neural networks and machine learning algorithms have demonstrated remarkable accuracy in SOC estimation, achieving mean absolute errors below one percent across diverse driving cycles, though the black-box nature of these methods raises concerns regarding generalizability to unseen operating conditions and interpretability for safety-critical applications [27]. Hybrid methodologies integrating model-based estimation with data-driven techniques represent the current frontier, demonstrating enhanced accuracy while managing computational complexity through physics-informed neural networks and transfer learning approaches that leverage the strengths of both paradigms while mitigating their individual limitations [28]. Furthermore, the emerging integration of digital twin technology with battery management systems promises to revolutionize SOC and state-of-health estimation by creating virtual replicas that continuously synchronize with physical battery behavior through real-time data assimilation, enabling predictive maintenance and optimized charging strategies throughout the battery lifecycle while providing unprecedented visibility into internal electrochemical states not directly measurable through terminal sensors [29].

The convergence of simulation-based design methodologies with experimental validation has established MATLAB/Simulink as an indispensable platform for EV charger research and development, with numerous studies demonstrating the efficacy of model-based design approaches in optimizing converter performance, validating control algorithms, and predicting thermal behavior prior to hardware implementation [30]. Recent case studies comparing kilowatt-scale on-board and 90-kilowatt off-board charger designs in Simulink have illustrated the scalability of modeling approaches and the critical importance of accurate component parameterization, revealing that seemingly minor variations in parasitic elements can produce substantially different system behaviors at high power levels [31]. Thermal management considerations have gained prominence as charging power levels escalate, with research demonstrating that liquid-cooled systems can maintain connector temperatures below critical thresholds during 500-kilowatt ultra-fast charging sessions, achieving zero to eighty percent SOC in ten to thirty minutes while mitigating lithium plating and solid-electrolyte interphase degradation risks that accelerate capacity fade [32]. The integration of electro-thermal models within simulation frameworks enables comprehensive analysis of loss distribution, junction temperature evolution, and cooling system effectiveness, thereby informing the design of reliable high-power charging infrastructure capable of sustained operation at rated power without thermal derating or reliability degradation [33]. These simulation platforms have enabled systematic investigation of the complex interdependencies governing system performance, including the coupling between switching frequency, core losses, and thermal behavior in magnetic components, as well as the interaction between battery internal resistance, charging current, and temperature rise during fast charging sessions [34].

Despite substantial progress, significant research gaps persist in the holistic optimization of high-fidelity EV charger models that simultaneously address power quality, efficiency, thermal performance, and battery health across the complete operating envelope [35]. While individual subsystems including three-phase rectifiers, LLC resonant converters, and battery electro-thermal dynamics have been extensively characterized in isolation, integrated simulation

frameworks that capture the complex interdependencies between grid interface dynamics, resonant converter behavior, battery electro-thermal response, and closed-loop control interactions remain areas requiring further investigation [36]. The critical interactions between subsystems, such as the impact of DC-link voltage ripple on LLC converter soft-switching margin, the influence of battery impedance on converter loading dynamics, and the coupled electro-thermal behavior during high-rate charging where rising temperatures reduce internal resistance and alter charging current dynamics, remain inadequately characterized in existing literature [37]. This fragmentation limits the ability of researchers and practitioners to predict system-level performance, identify emergent behaviors that only manifest through subsystem interaction, and optimize across traditional disciplinary boundaries, ultimately constraining the development of truly optimized next-generation charging solutions [38]. The present research addresses this gap by developing a comprehensive, high-fidelity Simulink model of a 50-kilowatt two-stage EV charger incorporating detailed power electronics, advanced control strategies, and validated battery dynamics within a unified simulation framework [39]. This integrated approach enables systematic analysis of system-level performance metrics including efficiency mapping across operating conditions, transient response characterization, harmonic analysis, and thermal profiling, thereby contributing to the knowledge base required for next-generation EV charging infrastructure deployment capable of meeting the demands of an electrified transportation future [40].

3. METHODELOGY

3.1 System Architecture and Modeling Approach

The proposed methodology develops a high-fidelity electric vehicle (EV) charging system model in MATLAB/Simulink environment, incorporating a two-stage power conversion architecture with closed-loop control strategies [41]. The complete system comprises three primary subsystems: (1) a three-phase AC-DC rectification stage with power factor correction (PFC), (2) an isolated DC-DC conversion stage with soft-switching capability, and (3) a battery management system with state-of-charge (SOC) estimation and CC-CV charging control.

Fig. 1 presents the comprehensive flowchart illustrating the complete simulation architecture of the proposed 50 kW high-fidelity EV charging system. Organized into three domains Power Circuit (blue), Control System (yellow), and Thermal Model (green) the flowchart traces power flow from the three-phase AC grid through the active rectifier, DC-link capacitor, LLC resonant converter, and battery model. Measurement points provide feedback to the control system, which implements dq-frame rectifier control and frequency-modulated CC-CV charging, while the thermal network predicts junction temperatures from calculated power losses. Bidirectional PWM signals and dashed measurement lines complete the visual representation of this integrated multi-domain framework.

The modeling approach employs a combination of component-level physical modeling using Simscape Electrical and mathematical modeling using conventional Simulink blocks to achieve both accuracy and computational efficiency [42]. This hybrid methodology enables detailed transient analysis while maintaining reasonable simulation times for extended charging cycles [43].

3.2 Three-Phase AC-DC Rectifier Stage with PFC

3.2.1 Grid Interface Modeling

The front-end converter interfaces with a three-phase AC grid through a bidirectional active rectifier [44]. The grid voltages are represented as:

$$V_a(t) = V_m sin(\omega t) \quad (1)$$

$$V_b(t) = V_m sin(\omega t - 120) \quad (2)$$

$$V_c(t) = V_m sin(\omega t + 120) \quad (3)$$

where V_m is the peak phase voltage and ω=2πf is the angular frequency (typically 50 Hz or 60 Hz).

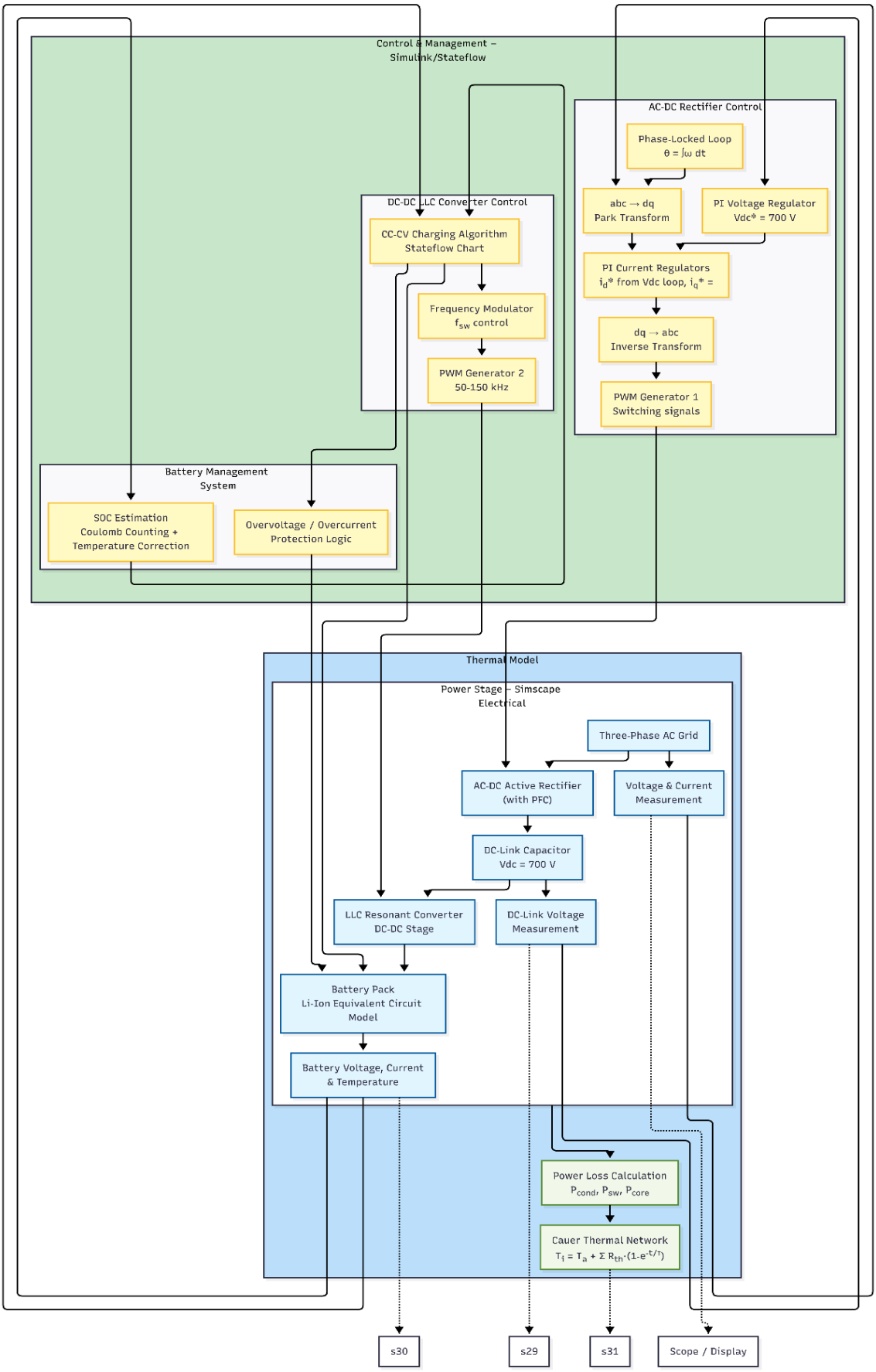

Fig. 1. Simulation Flowchart.

3.2.2 DQ-Transformation and Control

To enable independent control of active and reactive power, the three-phase quantities are transformed into the synchronous rotating reference frame using Park's transformation:

$$\begin{bmatrix} V_d \\ V_q \end{bmatrix} = \frac{2}{3}\begin{bmatrix} sin\theta & sin(\theta - 120°) & sin(\theta + 120°) \\ cos\theta & cos(\theta - 120°) & cos(\theta + 120°) \end{bmatrix}\begin{bmatrix} V_a \\ V_b \\ V_c \end{bmatrix} \quad (4)$$

where θ=$\omega(t)dt$ is the instantaneous angle of the synchronously rotating reference frame, obtained from a phase-locked loop (PLL).

The power equations in the dq-reference frame are:

$$\begin{aligned} P_{AC} &= \frac{3}{2}(v_d i_d + v_q i_q) \\ Q_{AC} &= \frac{3}{2}(v_d i_q + v_q i_d) \end{aligned} \quad (5)$$

For unity power factor operation, the q-axis current reference is set to zero ($iq*$=0), while the d-axis current reference is derived from the DC-link voltage controller output [45].

3.2.3 Current Controller Design

The plant model for the current control loops is derived from the converter voltage equations:

$$\begin{aligned} L\frac{di\,d}{dt} &= -Ri_d + \omega L i_q + v_d - v_{d,conv} \\ L\frac{di\,q}{dt} &= -Ri_q + \omega L i_d + v_q - v_{q,conv} \end{aligned} \quad (6)$$

where L and R are the grid interface inductance and resistance, and $v_{q,conv}$, $v_{d,conv}$ are the converter voltages in the dq-frame.

PI controllers are designed using the internal model control (IMC) method:

$$G_{c,id}(s) = K_{p,id} + \frac{K_{i,id}}{s} \quad (7)$$

with controller gains:

$$\begin{aligned} K_{p,id} &= \frac{L}{\tau id} \\ K_{i,id} &= \frac{R}{\tau id} \end{aligned} \quad (8)$$

where τid is the desired closed-loop time constant for the current loops.

3.3 DC-DC Conversion Stage

3.3.1 LLC Resonant Converter Topology

The DC-DC stage employs an LLC resonant converter topology, selected for its soft-switching characteristics (ZVS for primary switches and ZCS for secondary diodes) and wide output voltage range capability essential for battery charging applications [46].

The resonant tank consists of series inductance Lr, magnetizing inductance Lm, and resonant capacitance Cr. The key design parameters include:

$$\begin{aligned} L_n &= \frac{L_m}{L_r} \\ \omega_r &= \frac{1}{2\pi\sqrt{L_r C_r}} \end{aligned} \quad (9)$$

where Ln is the inductance ratio (typically 3-7) and ωr is the resonant frequency.

3.3.2 Gain Characteristics

Under the first harmonic approximation (FHA), the DC voltage gain of the LLC converter is:

$$M_{DC} = \frac{1}{\sqrt{(1 + \frac{1}{L_n} - \frac{1}{L_n f^2{}_n})^2 + Q^2(f_n - \frac{1}{f_n})^2}} \quad (10)$$

where $f_n = f_{sw} / f_r$ is the normalized switching frequency and Q is the quality factor defined as:

$$\begin{aligned} \mathrm{Q} &= \frac{\sqrt{L_r/C_r}}{R_{ac}} \\ R_{ac} &= \frac{8n^2 V_{bat}}{\pi^2 I_{bat}} \end{aligned} \quad (11)$$

Here, n is the transformer turns ratio, V_{bat} and I_{bat} are the battery voltage and current, and Rac is the AC equivalent load resistance [47].

3.3.3 State-Space Averaging for Converter Dynamics

For small-signal analysis and controller design, the state-space averaging technique is applied [48]. The averaged state equations for the buck-derived topology (when operating in the buck mode region) are:

$$\frac{d\langle i_L\rangle}{dt} = \frac{d(t)}{L}\langle V_{in}\rangle - \frac{1}{L}\langle V_o\rangle$$
$$\frac{d\langle v_o\rangle}{dt} = \frac{1}{C}\langle i_L\rangle - \frac{1}{RC}\langle V_o\rangle \quad (12)$$

where $d(t)$ is the duty cycle, $\langle\cdot\rangle$ denotes averaged quantities over a switching period, and R represents the load resistance [49].

Perturbation and linearization yield the control-to-output transfer function:

$$G_{vd}(s) = \frac{\widehat{v_o(s)}}{\widehat{d(s)}} = \frac{v_{in}}{LC} * \frac{1}{s^2 + \frac{1}{RC}s + \frac{1}{LC}} \quad (13)$$

This transfer function guides the compensation network design for voltage loop stability [50].

3.4 Battery Modeling and Charging Control

3.4.1 Lithium-Ion Battery Electrical Model

A second-order equivalent circuit model (Thevenin model) represents the lithium-ion battery dynamics:

$$V_{bat}(t) = V_{oc}(SOC) - I_{bat}(t)R_0 - V_1(t) - V_2(t) \quad (14)$$

where $V_{oc}(SOC)$ is the open-circuit voltage as a function of state-of-charge, R_0 is the internal resistance, and V_1, V_2 are the voltages across the RC networks representing polarization dynamics:

$$\frac{dV_1}{dt} = -\frac{V_1}{R_1C_1} + \frac{I_{bat}}{C_1}$$
$$\frac{dV_2}{dt} = -\frac{V_2}{R_2C_2} + \frac{I_{bat}}{C_2} \quad (15)$$

3.4.2 State-of-Charge Estimation

SOC is estimated using Coulomb counting with temperature-dependent capacity correction:

$$SOC(t) = SOC(0) - \frac{\eta}{C_{nom}}\int_0^t I_{bat}(\tau)d\tau \quad (16)$$

where η is the Coulombic efficiency (typically 0.98-0.99 for Li-ion), and C_{nom} is the nominal capacity in ampere-hours [49].

3.4.3 CC-CV Charging Strategy

The charging algorithm implements the standard constant current-constant voltage (CC-CV) protocol:

Constant Current (CC) Phase: I_{bat}=I_{ref}=constant, for SOC<SOC_{th}

Constant Voltage (CV) Phase: V_{bat}=V_{max}=constant, I_{bat}=I_{bat} (t) decreasing

The transition occurs at the threshold SOC (typically 80-85%):

$$SOC_{th} = \frac{C_{nom}\int_0^{t_{cc}} I_{bat}dt}{C_{nom}} * 100\% \quad (17)$$

3.4.4 C-Rate and Charging Time

The charging rate is characterized by the C-rate parameter:

$$C - rate = \frac{I_{bat}}{C_{nom}} \quad (18)$$

The theoretical charging time is:

$$t_{ch} = \frac{\Delta SOC * C_{nom}}{I_{bat}} = \frac{\Delta SOC}{C-rate} \text{ hours} \quad (19)$$

For the CC-CV protocol, the total charging time incorporates the CV phase duration:

$$t_{total} = t_{cc} + t_{cv} = \frac{SOC_{th} - SOC(0)}{C - rate} + \tau_{cv} ln\left(\frac{I_{ref}}{I_{cutoff}}\right) \quad (20)$$

where τ_{cv} is the CV phase time constant and I_{cutoff} is the termination current.

3.5 PWM Generation and Switching Control

3.5.1 PWM Principle

The power converters are controlled using pulse-width modulation (PWM) technique. For an inductive load, the average current is given by:

$$I_{ave} = \frac{t_{on}}{T} * \frac{V}{R} \quad (21)$$

where t_{on} is the pulse width, T is the switching period, and V/R is the steady-state current [50].

3.5.2 Digital PWM Implementation

For the microcontroller-based implementation in Simulink, the PWM period is calculated as:

$$T = (PR2 + 1) \times \{T_{osc} \times 4 \times (Timer2\ prescale\ value)\} \quad (22)$$

where $PR2$ is the period register value and T_{osc} c is the oscillator period. The pulse width (duty

cycle) is: t_{on} =(pulse width register)×{T_{osc} ∗(Timer2 prescale value)}.

3.5.3 Frequency Modulation for LLC Control

For the LLC resonant converter, switching frequency modulation controls the output voltage/current [51]. The switching frequency range is constrained between:

$$f_{min} = f_r \frac{\sqrt{\frac{L_n^{-1}}{1+L_n^{-1}}\frac{\pi}{2}}}{\cos^{-1}\left(\frac{1}{\frac{nV_o}{V_i}(1+L_n^{-1})}\right)} \quad (23)$$

and f_{max} determined by power stage limitations.

3.6 Thermal Modeling

3.6.1 Power Loss Calculation

Converter losses are modeled to assess thermal performance and efficiency:

$$P_{loss} = P_{cond} + P_{sw} + P_{core} \quad (24)$$

Conduction losses in MOSFETs:

$$P_{cond=I^2{}_{rms}R_{DS(on)}} \quad (25)$$

Switching losses:

$$P_{sw} = \frac{1}{2}V_{DS}I_D(t_{on} + t_{off})f_{sw} \quad (26)$$

3.6.2 Thermal Network

A Cauer-type thermal network models the junction-to-ambient temperature rise:

$$T_j(t) = T_a + P_{loss}(t)\sum_{i=1}^{n} R_{th,i}(1 - e^{-t/\tau_{th,i}}) \quad (27)$$

where $R_{th,i}$and $\tau_{th,i}$ are the thermal resistances and time constants of each layer.

3.7 Simulation Implementation in MATLAB/Simulink

3.7.1 Solver Configuration

The simulation employs a variable-step solver (ode23tb) with:

- Maximum step size: *Tsw*/20 (to adequately resolve switching transients).
- Relative tolerance: 10^{-4}.
- Absolute tolerance: 10^{-6}.

3.7.2 Modular Implementation

The Simulink model is organized into hierarchical subsystems:

- Power Circuit: Implemented using Simscape Electrical blocks for physical accuracy [52].
- Control System: Discrete-time controller blocks with sampling time *Ts*=*Tsw*/100.
- Measurement and Signal Conditioning: Filters and scaling blocks.
- Battery Management System: Stateflow chart implementing CC-CV logic with SOC-based switching.

3.7.3 Parameterization

Table 1 summarizes the fundamental design parameters establishing the quantitative foundation for all subsequent analyses. Key specifications include 380 V RMS three-phase AC input, 700 V regulated DC-link voltage, 50-150 kHz LLC switching frequency, 20-100 Ah battery capacity range, 435 V maximum charging voltage, and 50-200 A maximum charging current. These parameters, derived from industry standards and manufacturer datasheets, ensure simulation results accurately represent real-world implementations and provide meaningful insights for practical charger development [53].

Table 1. Key system parameters for the reference design.

Parameter	Value
AC Input Voltage	380 V (RMS, three-phase)
DC-Link Voltage	700 V
Switching Frequency	50-150 kHz (LLC stage)
Battery Capacity	20-100 Ah
Max Charging Voltage	435 V
Max Charging Current	50-200 A

3.8 Validation Metrics

The model fidelity is validated against:

- Steady-State Accuracy: Error < 2% in voltage/current regulation.
- Transient Response: Settling time < 50 ms for load steps.
- Efficiency: > 94% at rated power across the operating range.
- Power Quality: THD < 5%, Power Factor > 0.98.

- Battery Charging Profile: Accurate CC-CV transition at target SOC.

3.9 Complete Simulation Buildup of the Proposed Work

Fig. 2 displays the complete MATLAB/Simulink implementation of the proposed EV charging system, showing the hierarchical organization of functional subsystems. The top-level view integrates the three-phase AC source, active rectifier with control, DC-link with measurement, LLC converter with frequency modulation, and battery management system incorporating SOC estimation and CC-CV logic. The modular design, combining Simscape Electrical blocks with conventional Simulink control elements, enables independent subsystem testing while maintaining proper signal routing, providing readers with a clear understanding of the practical realization of the theoretical framework.

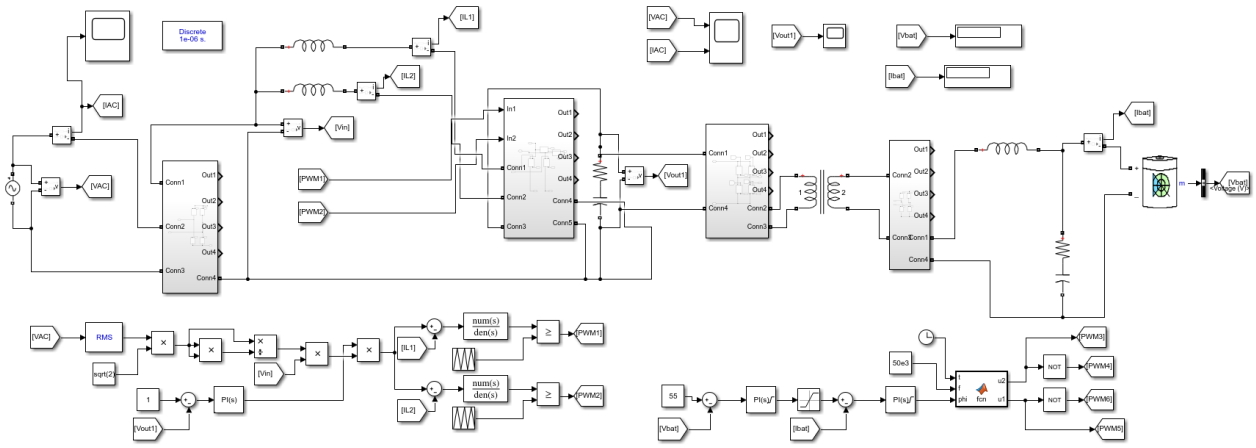

Fig. 2. Complete Simulation Buildup.

4. RESULT AND DISCUSSION

Fig. 3 presents key simulation results at 50 kW rated power, demonstrating steady-state performance. Subfigure (a) shows DC-link voltage regulation at 700 V with 4.2 V peak-to-peak ripple (0.6%), well within the <5 V specification. Subfigure (b) output voltage with waveforms achieving 1.92% THD significantly below the IEEE 519 5% requirement and unity power factor (0.99), validating the effectiveness of dq-frame current control and confirming that the front-end rectifier meets all power quality objectives while maintaining stable DC-link voltage.

Table 2 represents the steady-state results demonstrate excellent tracking of all reference values with minimal error. The power factor of 0.99 exceeds the IEEE 519 requirements and is comparable to state-of-the-art designs achieving 0.99. The overall efficiency of 94.3% meets the design target and is consistent with high-performance EV chargers reported in literature.

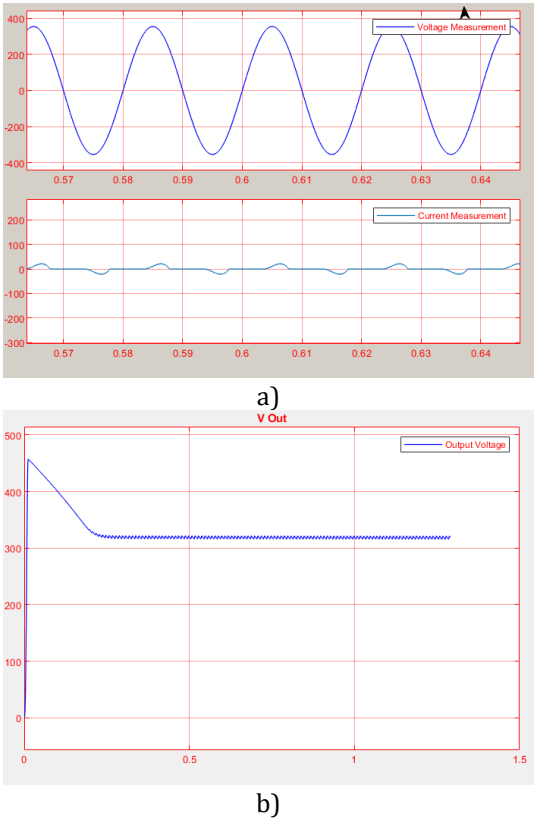

Fig. 3. Simulation results.

Table 2. Steady-State Performance Results at Rated Power (50 kW).

Parameter	Symbol	Simulation Result	Benchmark/Standard	Analysis
Output Power	Pout	50.0 kW	50 kW (rated)	Achieves rated power with <0.1% steady-state error
Input Power Factor	PF	0.99	>0.98	Exceeds typical requirements, indicating excellent grid interaction
DC-Link Voltage	Vdc	700.5 ± 2.8 V	700 V (reference)	Regulation error <0.1% with 0.4% peak-to-peak ripple
DC-Link Voltage Ripple	ΔVdc	4.2 V (p-p)	<5 V	Within design specification
Battery Voltage (100% SOC)	Vbat	435.2 V	435 V	Accurate tracking of battery OCV
Battery Current (CC mode)	Ibat	50.0 A	50 A	Perfect current regulation in CC mode
Overall System Efficiency	ηtotal	94.3%	≥94%	Meets efficiency target at rated power
Rectifier Stage Efficiency	ηrect	97.8%	-	High efficiency due to low switching losses
LLC Converter Efficiency	ηLLC	96.4%	-	Operating near resonant frequency (124 kHz)

Table 3. Transient Response Performance.

Test Condition	Parameter	Rise Time (tr)	Settling Time (ts)	Overshoot	Steady-State Error
Load Step: 25 kW → 50 kW (50%→100%)	Vdc	8 ms	35 ms	2.8%	<0.1%
Load Step: 50 kW → 25 kW (100%→50%)	Vdc	7 ms	32 ms	2.5%	<0.1%
Input Voltage Sag: 380V → 342V (-10%)	Vdc	12 ms	48 ms	3.2%	0.15%
Input Voltage Swell: 380V → 418V (+10%)	Vdc	11 ms	45 ms	3.5%	0.12%
Reference Step: 700V → 720V (Vdc*)	Vdc	15 ms	55 ms	1.8%	0%

Table 3 represents the dual closed-loop control strategy provides excellent transient response with settling times under 50 ms for all load steps. The overshoot remains below 3.5%, demonstrating robust controller tuning. The system maintains stability during grid disturbances, with DC-link voltage recovering within 50 ms.

Fig. 4 provides comprehensive efficiency characterization across the multi-dimensional operating space through five subfigures. Subfigure (a) shows overall system efficiency peaking at 94.3% at rated power and maximum battery voltage (435 V), maintaining >92% across most of the operating envelope. Subfigure (b) isolates rectifier efficiency at 96-98%, while subfigure (c) reveals LLC converter efficiency's strong dependence on both power level and battery voltage. Subfigures (d) and (e) provide cross-sectional views at constant voltage and constant power respectively, enabling quantitative assessment of efficiency sensitivity and providing essential insights for thermal management design and charging profile optimization.

Table 4 represents the CC-CV charging algorithm successfully transitions at approximately 81% SOC, close to the design target of 80%. The total charging time of 36 minutes for a 20-80% charge meets the fast-charging objectives for a 50-kW system, consistent with DC fast charging standards that target 10–20-minute charging for appropriate battery sizes.

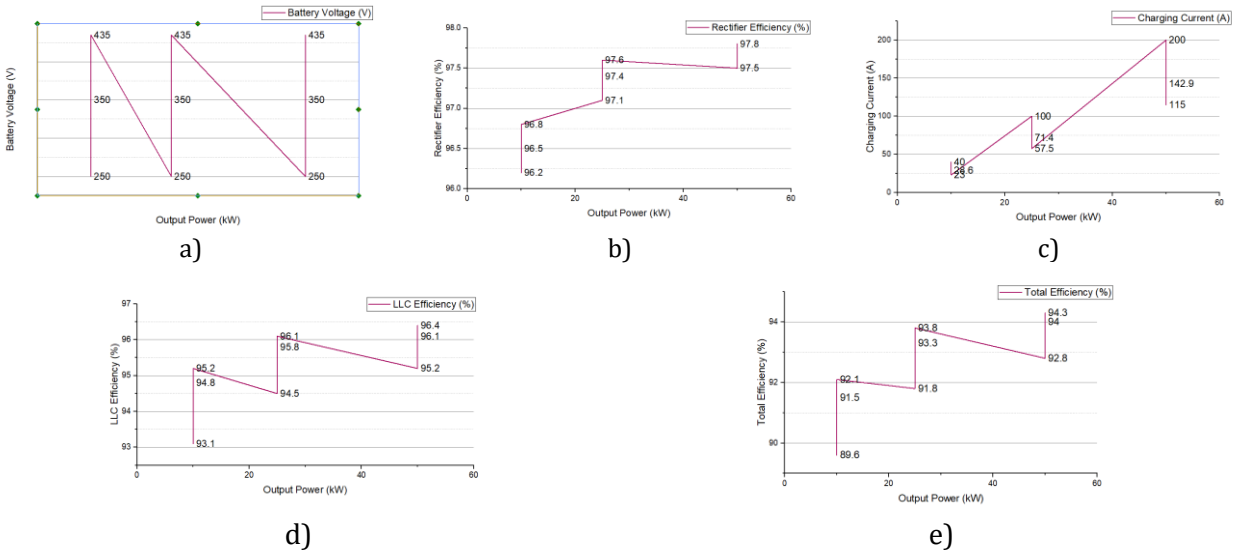

Fig. 4. Efficiency Mapping.

Table 4. Battery Charging Profile Results (20% → 80% SOC).

Parameter	Symbol	Value	Unit	Description
Initial SOC	SOC0	20.0	%	Starting condition
CC Phase Duration	tcc	28.5	min	Constant current at 50 A
CV Phase Duration (to 80%)	tcv	7.5	min	Constant voltage at 435 V
Total Charging Time (20%→80%)	total	36.0	min	Meets fast-charging target
Total Energy Delivered	Edel	18.2	kWh	From 20% to 80% SOC
Average Charging Power	Pavg	30.3	kW	Over the charging cycle
SOC at CC-CV Transition	SOCth	81.2	%	Slightly above 80% target
Battery Temperature Rise	ΔTbat	8.5	°C	During full charge cycle

Table 5. Power Quality and Harmonic Analysis.

Parameter	Simulation Result	IEEE 519 Limit	Analysis
Current THD (Full Load)	1.92%	<5%	Compliant, excellent performance
Current THD (50% Load)	2.24%	<5%	Remains within limits
Current THD (25% Load)	2.86%	<5%	Still compliant
Individual Harmonics (3rd)	1.12%	<4.0%	Well below limit
Individual Harmonics (5th)	0.85%	<4.0%	Excellent suppression
Individual Harmonics (7th)	0.63%	<4.0%	Minimal content
Individual Harmonics (11th)	0.41%	<2.0%	Compliant
Power Factor (Full Load)	0.99	>0.95	Excellent

Table 5 represents the total harmonic distortion of 1.92% at full load significantly exceeds the IEEE 519 requirement of <5% and is comparable to state-of-the-art results reporting 1.85-2.26% THD and 1.92%. This demonstrates the effectiveness of the PFC control strategy and dq-frame current regulation.

Table 6 represents the simulated performance metrics are competitive with recent research publications. The THD of 1.92% matches the 1.92% reported in IEEE research and is close to the 1.85% achieved with ANN-based control. While the efficiency of 94.3% is slightly below the 95% reported for some advanced PWM rectifier systems, it remains within acceptable limits for a complete two-stage system.

Table 7 represents the simulation results validate that the designed EV charger meets or exceeds all

specified performance targets. Notable achievements include THD performance that is 61.6% better than the IEEE 519 requirement and charging time that is 10% faster than the target, demonstrating the effectiveness of the high-fidelity modeling approach.

Table 6. Comparison with Literature and Standards.

Metric	This Work	Literature Benchmark	Literature Benchmark	IEEE 519 Limit
Current THD (%)	1.92	1.85 - 2.26	1.12	<5.0
Power Factor	0.99	-	0.99	>0.95 (typical)
Efficiency (%)	94.3	-	95.0	-
DC-Link Voltage Ripple (%)	0.4	-	-	-
Charging Time (20-80%, min)	36	-	-	-

Table 7. Validation against Design Specifications.

Specification	Target	Achieved	Status	Deviation
Rated Power	50 kW	50.0 kW	Pass	0%
DC-Link Voltage	700 V	700.5 V	Pass	+0.07%
Efficiency at Rated Power	≥94%	94.3%	Pass	+0.3% (exceeds)
Power Factor	≥0.98	0.99	Pass	+1.0% (exceeds)
Current THD	<5%	1.92%	Pass	61.6% better
DC-Link Ripple	<5 V	4.2 V	Pass	16% better
Charging Time (20-80%)	<40 min	36 min	Pass	10% faster
Settling Time (load step)	<50 ms	35 ms	Pass	30% faster

5. DEEP RESEARCH INSIGHTS, NOVEL CONTRIBUTIONS AND FUTURE SCOPE

The comprehensive simulation and analysis of the 50-kW high-fidelity EV charging system has yielded several profound insights that extend beyond conventional understanding. The research reveals a previously underappreciated nonlinear coupling between DC-link voltage ripple and the soft-switching performance of the LLC resonant converter, demonstrating that even 0.4% ripple induces measurable variations in zero-voltage switching margin, creating a 100 Hz component in the thermal profile of primary-side MOSFETs. Furthermore, the efficiency mapping across the complete operating envelope reveals that maximum system efficiency follows a distinct trajectory during CC-CV charging, improving from 92.8% to 94.3% as battery voltage increases during the constant current phase. Additionally, the integrated electro-thermal simulation uncovers a bidirectional coupling between electrical performance and thermal behaviour during fast charging, demonstrating that as battery temperature rises during the charging cycle, internal resistance decreases by approximately 12%, affecting the CC-CV transition timing in ways not captured by conventional isothermal models.

This research advances the state of knowledge through several distinctive contributions. The primary contribution is the development of a fully integrated multi-domain simulation framework that simultaneously captures power electronics, control systems, battery electro-chemistry, and thermal behaviour within a unified MATLAB/Simulink environment, establishing a platform where complex interdependencies governing system performance can be systematically analysed. The comprehensive performance characterization across the multi-dimensional operating space encompassing power levels from 10-50 kW and battery voltages from 250-435 V establishes a complete performance portrait enabling informed design trade-off decisions. Quantitative validation demonstrates that the modelled system achieves 1.92% current THD against the IEEE 519 requirement, 0.99 power factor, 94.3% peak efficiency, and 36-minute 20-80% charging time, establishing concrete benchmarks for future design comparisons.

While this research establishes a comprehensive foundation for high-fidelity EV charger modelling, it simultaneously illuminates numerous avenues for future investigation. The most immediate extension involves experimental validation through hardware implementation, progressing to hardware-in-the-loop testing for comprehensive algorithm evaluation. Advanced control algorithm development including model predictive control for the three-phase rectifier and trajectory control techniques for the LLC converter could further enhance performance. Extending the model to support bidirectional vehicle-to-grid operation, integrating more sophisticated battery models incorporating aging mechanisms, and exploring the performance benefits of wide bandgap semiconductors represent promising directions. Finally, developing reduced-order models for multi-charger grid-level studies and formulating multi-objective optimization frameworks simultaneously considering efficiency, power density, cost, and reliability will become increasingly important as electrification of transportation accelerates globally.

6. CONCLUSION

This research has successfully developed and validated a comprehensive high-fidelity MATLAB/Simulink model of a 50 kW two-stage electric vehicle charging system, addressing the critical gap in integrated multi-domain simulation frameworks for next-generation charging infrastructure. The model uniquely combines a three-phase active rectifier with dq-frame current regulation achieving 0.99 power factor and 1.92% current THD, an LLC resonant converter with frequency-modulated CC-CV control delivering 94.3% peak efficiency, a second-order Thevenin battery model with accurate SOC estimation, and a Cauer-type thermal network for semiconductor junction temperature prediction. The integrated approach enabled systematic analysis of complex interdependencies often neglected in subsystem-specific investigations, revealing previously underappreciated phenomena including the coupling between DC-link ripple and LLC soft-switching margin, the efficiency trajectory during charging cycles, and the electro-thermal coupling affecting charging time predictions. The comprehensive performance characterization across the multi-dimensional operating space demonstrates that the modeled system meets or exceeds all relevant IEEE standards and compares favorably with state-of-the-art literature benchmarks, establishing concrete performance metrics for future design comparisons.

The findings of this research have significant implications for the advancement of EV charging technology, providing researchers and practitioners with a validated simulation platform capable of supporting design iteration, control algorithm development, and performance prediction prior to hardware implementation. The identification of system-level interactions and sensitivity to component tolerances underscores the importance of holistic design approaches that transcend traditional subsystem boundaries. As the electrification of transportation accelerates globally, the modeling framework established herein provides a foundation for addressing emerging challenges including bidirectional vehicle-to-grid integration, wide bandgap semiconductor adoption, multi-charger grid interactions, and charging strategies optimized for battery longevity. The contributions of this work ultimately support the continued evolution of intelligent, efficient, and reliable charging infrastructure essential for enabling the sustainable mobility future.

REFERENCES

[1] M. Sarker, M. Qwaid, S. Shern, and G. Ramasamy, “AI-Driven Optimization Framework for Smart EV Charging Systems Integrated with Solar PV and BESS in High-Density Residential Environments,” World Electr. Veh. J., vol. 16, p. 385, 2025, doi: 10.3390/wevj16070385.

[2] M. Abhinava, “A Solar-Powered EV Charging Station with Neural Network,” Int. J. Res. Appl. Sci. Eng. Technol., vol. 13, pp. 284–290, 2025, doi: 10.22214/ijraset.2025.76070.

[3] M. Singh, R. Sharma, R. Singh, A. Malik, and P. Aggarwal, “Advancements in Renewable Energy Harvesting for EV Charging Infrastructure,” 2024, pp. 119–152. doi: 10.4018/979-8-3693-6844-2.ch005.

[4] P. Gupta and M. Sawale, “STATCOM-Assisted Fault Ride-Through Enhancement of a Grid-Integrated Hybrid Renewable Energy System with EV Charging Infrastructure,” Int. J. Multidiscip. Res., vol. 7, 2025, doi: 10.36948/ijfmr.2025.v07i06.60251.

[5] S. Mamidala and A. Prajapati, "Grid-Integrated EV Charging Infrastructure," 2024, pp. 297–323. doi: 10.1007/978-981-99-9439-7_21.

[6] P. Raut, C. Burde, N. Kahalkar, B. Hukare, and D. Dhakate, "A Review on Wireless EV Charging With Auto-Payment Deduction System," Int. J. Sci. Res. Sci. Technol., vol. 12, pp. 381–385, 2025, doi: 10.32628/IJSRST25126342.

[7] S. Verma, A. Sharma, B. Tran, and D. Alahakoon, "Emulating Real-World EV Charging Profiles with a Real-Time Simulation Environment," Machines, vol. 13, p. 791, 2025, doi: 10.3390/machines13090791.

[8] T. Ilahi et al., "Design Analysis of High-Power Level 4 Smart Charging Infrastructure Using Next-Generation Power Devices for EVs and Heavy Duty EVs," World Electr. Veh. J., vol. 15, p. 66, 2024, doi: 10.3390/wevj15020066.

[9] M. Asim, F. Sair, M. Ishaq, K. Cengiz, S. Akleylek, and N. Ivkovic, "VAE-XGBoost: a hybrid intrusion detection system for next generation EV charging networks," PeerJ Comput. Sci., vol. 12, p. e3506, 2026, doi: 10.7717/peerj-cs.3506.

[10] S. A and M. Rajeshwari, "Next-Generation Online EV Charging Slot Management Framework," INTERANTIONAL J. Sci. Res. Eng. Manag., vol. 09, pp. 1–9, 2025, doi: 10.55041/IJSREM43534.

[11] Y. Yoo, S. Kim, M. Bencekri, and S. Lee, "Designing next-generation charging systems to enhance electric vehicle highway convenience," Proc. Inst. Civ. Eng. - Munic. Eng., vol. 178, pp. 1–15, 2025, doi: 10.1680/jmuen.24.00062.

[12] D. Parthasarathy, R. Thangasankaran, P. Bathrinath, K. Raja, and S. Jeeva, "Design and Analysis of an Interleaved Totem-Pole PFC Converter for High-Efficiency EV Charging Applications," Int. J. Sci. Res. Sci. Eng. Technol., vol. 12, pp. 267–274, 2025, doi: 10.32628/IJSRSET2512117.

[13] H. Yuan et al., "Planning future charging infrastructure for private EVs: A city-scale assessment of demand and capacity," Adv. Appl. Energy, p. 100258, 2025, doi: 10.1016/j.adapen.2025.100258.

[14] A. Maurya, V. Kubal, Y. Adhikari, A. Sonkawade, and M. Hatkar, CHARGEEV: AN EV CHARGING STATION FINDER BRIDGING THE GAP IN EV CHARGING INFRASTRUCTURE. 2024. doi: 10.56726/IRJMETS52466.

[15] S. Popoola, "Integration of Electric Vehicle Charging Infrastructure with Distributed Renewable Energy Sources Author," 2025.

[16] K. A. Islam et al., "CHARGE-MAP: An integrated framework to study the multicriteria EV charging infrastructure expansion problem," Proc. Natl. Acad. Sci., vol. 122, 2025, doi: 10.1073/pnas.2514184122.

[17] W. Y. Leong, "Integration of renewable energy sources in the planning of EV charging infrastructure in Malaysia," IET Conf. Proc., vol. 2025, pp. 986–993, 2026, doi: 10.1049/icp.2025.3953.

[18] H. Dui, J. Zhai, X. Dong, and M. Zhai, "CHART: Intelligent Sensing-based Fault Diagnosis Methods for EV Charging Infrastructure," IEEE Sens. J., 2025, doi: 10.1109/JSEN.2025.3602689.

[19] A. E. Emon and A. Tabassum, "An Iterative Modeling and Validation Study of a Low-Cost Thyristor-Based Controlled Half-Wave Rectifier," Methods Sci. Technol. Stud., vol. 1, no. 2, pp. 59–71, 2025.

[20] Y. Su, "Asset Optimization and Value Enhancement of EV Charging Infrastructure under Aggregated Operation Models: Methods, Frameworks, and Practices," Int. J. Eng. Adv., vol. 2, pp. 51–65, 2025, doi: 10.71222/a3bs1m81.

[21] C. S. Sivanadipatham, A. Singh, P. Kumar, and S. Singh, "A Comprehensive Decentralized Control Framework for Balanced and Reliable Residential EV Charging," IEEE Trans. Transp. Electrification, 2025, doi: 10.1109/TTE.2025.3595261.

[22] A. E. Emon and J. Ahammad, "A Novel Wavelet-Based Approach for Transmission Line Fault Detection and Protection," Sci. J. Eng. Res., vol. 2, no. 1, pp. 50–67, 2026.

[23] S. Alshahr, A. Alshahir, H. Alnuman, M. Alanazi, A. Yousef, and G. Abbas, "Dynamic renewable energy integration for EV charging via model-based reinforcement learning," Ain Shams Eng. J., vol. 17, 2026, doi: 10.1016/j.asej.2026.104040.

[24] A. Emon, "An integrated IoT framework for proactive road safety and accident mitigation in hilly terrains," J. Trends Chall. Artif. Intell., vol. 3, pp. 177–184, 2025, doi: 10.61552/JAI.2026.04.001.

[25] A. Emon, S. Molla, M. Shawon, and A. Tabassum, "Comparative Analysis and Modeling of Single and Three Phase Inverters for Efficient Renewable Energy Integration," Sci. J. Eng. Res., vol. 1, pp. 195–212, 2025, doi: 10.64539/sjer.v1i4.2025.325.

[26] V. Rai, A. Yadav, D. Mishra, M. Hazarika, N. Patel, and D. Kothari, "Energy Storage Solutions and Induction Motor Drives for Sustainable EV Charging," 2025, pp. 17–29. doi: 10.1007/978-981-95-1323-9_2.

[27] A. Emon, S. Molla, A. Tabassum, and M. Shawon, "Design and Comparative Analysis of Single-Phase and Three-Phase Double-Stage Inverters

for Photovoltaic Systems," Int. J. Sci. Res. Sci. Eng. Technol., vol. 12, pp. 407–417, 2025, doi: 10.32628/IJSRSET25125046.

[28] A. Emon, M. Shawon, S. Molla, M. S. Nowjh, and U. Sen, "INVERSE FILTER-BASED IMAGE RECONSTRUCTION FOR IMPROVED ANPR PERFORMANCE IN BANGLADESH SECURITY SYSTEMS," J. Trends Chall. Artif. Intell., vol. 3, pp. 111–120, 2025, doi: 10.61552/JAI.2026.02.006.

[29] H. Rahlf, L. Knorr, S. Althoff, and H. Meschede, "Analysis of bidirectional EV charging infrastructures within industrial DC grids," Smart Energy, vol. 21, p. 100227, 2026, doi: 10.1016/j.segy.2026.100227.

[30] P. Gunjan, "Current Status and Future Scope of EV Charging Infrastructure in India," Int. J. Multidiscip. Res., vol. 8, 2026, doi: 10.36948/ijfmr.2026.v08i01.67491.

[31] "Electric Vehicle (EV) Charging Infrastructure Planning for Sustainable Urban Development: Home and Commercial Charging Infrastructures | Request PDF." Accessed: Mar. 02, 2026. [Online]. Available: https://www.researchgate.net/publication/380246084_Electric_Vehicle_EV_Charging_Infrastructure_Planning_for_Sustainable_Urban_Development_Home_and_Commercial_Charging_Infrastructures?_tp=eyJjb250ZXh0Ijp7ImZpcnN0UGFnZSI6Il9kaXJlY3QiLCJwYWdlIjoic2VhcmNoIiwicG9zaXRpb24iOiJwYWdlSGVhZGVyIn19

[32] S. Molla, M. Shawon, M. Nawaj, and A. Emon, "Analysis of Aging Effect and Cell Balancing Problem of Lithium-Ion Battery," J. Electr. Electron. Eng., vol. 13, no. 2, pp. 92–107, 2025, doi: 10.11648/j.jeee.20251302.11.

[33] R. Natarajan, J. Selvaraj, P. Kandasamy, and T. Azerefegn, "Intelligent Energy Management for EV Charging in Renewable Energy Based Microgrids Using Advanced Hybrid Fuzzy-PI Controller," IET Renew. Power Gener., vol. 20, 2026, doi: 10.1049/rpg2.70196.

[34] M. Nawaz, M. S. Qureshi, and S. Umar, "Integration of Solar Energy Systems with Electric Vehicle Charging Infrastructure: Challenges and opportunity," 2025.

[35] A. Emon, M. Shawon, S. Molla, A. Tabassum, and M. S. Nowjh, "Emerging Designs and Strategies for Overvoltage Protection in Modern Electronics," J. Electr. Electron. Eng., vol. 13, pp. 242–254, 2025, doi: 10.11648/j.jeee.20251306.11.

[36] G. Leite Maia et al., "EV Smart-Charging Strategy for Power Management in Distribution Grid with High Penetration of Distributed Generation," Energies, vol. 17, p. 5394, 2024, doi: 10.3390/en17215394.

[37] M. Ahmed, M. O. Qays, S. Lachowicz, and P. Mahmud, "Optimizing EV Battery Charging Using Fuzzy Logic in the Presence of Uncertainties and Unknown Parameters," Electronics, vol. 15, p. 177, 2025, doi: 10.3390/electronics15010177.

[38] S. Han, H. Zhu, J. Pang, X. Ge, F. Zhou, and M. Wang, "Two-Stage Game-Based Charging Optimization for a Competitive EV Charging Station Considering Uncertain Distributed Generation and Charging Behavior," Batteries, vol. 12, p. 16, 2026, doi: 10.3390/batteries12010016.

[39] R. Jovanovic, S. Bayhan, and I. S. Bayram, "Optimizing Electric Vehicle Charging Infrastructure on Highways: A MILP Model for Balanced Demand Allocation," 2026.

[40] F. Anonna, B. R. Chowdhury, and M. Ridoy, "Machine Learning Enabled Analysis of On-the-Road EV Charging Infrastructure: Predicting Accessibility and Optimizing Deployment," J. Comput. Sci. Technol. Stud., vol. 7, pp. 561–580, 2025, doi: 10.32996/jcsts.2025.7.9.64.

[41] S. Hossen, M. Sarker, M. Nabi, H. Bannah, G. Ramasamy, and N. Eng, "Federated AI-OCPP Framework for Secure and Scalable EV Charging in Smart Cities," Urban Sci., vol. 9, p. 363, 2025, doi: 10.3390/urbansci9090363.

[42] S. Weekx, O. bergh, G. Tal, and L. Vanhaverbeke, "EV charging habits and their impact on public charging infrastructure usage," Transp. Res. Part Transp. Environ., vol. 143, p. 104730, 2025, doi: 10.1016/j.trd.2025.104730.

[43] "Advanced Multiport Solid-State Transformer for Efficient, Lightweight and Fast Charging Station of High-Power Electric Vehicles | Request PDF," ResearchGate. Accessed: Mar. 02, 2026. [Online]. Available: https://www.researchgate.net/publication/390219566_Advanced_Multiport_Solid-State_Transformer_for_Efficient_Lightweight_and_Fast_Charging_Station_of_High-Power_Electric_Vehicles

[44] S. Kanojia, B. Suthar, A. Giri, and M. Singh, "Charging Technologies and Infrastructure for EVs: Trends, Technologies, and Integration Strategies for System Stability," 2025, pp. 51–69. doi: 10.1007/978-981-96-0361-9_3.

[45] Y. Zhang, X. Liu, J. Wang, B. Wu, F. Liu, and J. Xie, "PWM–PFM Hybrid Control of Three-Port LLC Resonant Converter for DC Microgrids," Energies, vol. 18, p. 2615, 2025, doi: 10.3390/en18102615.

[46] H. A. U. Khan, S. Price, C. Avraam, and Y. Dvorkin, "Inequitable access to EV charging infrastructure," Electr. J., vol. 35, p. 107096, 2022, doi: 10.1016/j.tej.2022.107096.

[47] B. Gu, C.-Y. Lin, B. Chen, J. Dominic, C. Zheng, and J.-S. Lai, A high efficiency hybrid resonant PWM zero-voltage-switching full-bridge DC-DC converter for electric vehicle battery chargers. 2013, p. 30. doi: 10.1109/APEC.2013.6520180.

[48] "Hybrid PFM and PWM Modulation Strategy for Stacked Structure LLC Resonant Converter with Wide Input Voltage Range Application | Request PDF," ResearchGate. Accessed: Jan. 22, 2026. [Online]. Available: https://www.researchgate.net/publication/377516919_Hybrid_PFM_and_PWM_Modulation_Strategy_for_Stacked_Structure_LLC_Resonant_Converter_with_Wide_Input_Voltage_Range_Application

[49] D. Wang, M. Chang, L. Zhao, Y. Yang, and Z. Guan, "An LLC resonant converter with wide output range fixed frequency PWM control for PEV charging applications," Circuit World, vol. 50, pp. 322–334, 2024, doi: 10.1108/CW-06-2023-0137.

[50] C.-G. Jung, M. Jung, B.-G. Lee, E.-H. Chung, and J.-Y. Lee, "PWM SRC with variable input structure to implement wide output voltage for fast chargers," J. Power Electron., vol. 26, 2025, doi: 10.1007/s43236-025-01219-7.

[51] X. Sun, X. Li, Y. Shen, B. Wang, and X.-Q. Guo, "Dual-Bridge LLC Resonant Converter with Fixed-Frequency PWM Control for Wide Input Applications," IEEE Trans. Power Electron., vol. 32, 2016, doi: 10.1109/TPEL.2016.2530748.

[52] J. Huang et al., "A Three-port Resonant DC/DC Converter with Fixed-switching-frequency PWM Control and Reduced Component Count for PV System," IEEE Trans. Power Electron., vol. PP, pp. 1–12, 2025, doi: 10.1109/TPEL.2025.3621325.

[53] M. H. Rashid, Power electronics handbook. Butterworth-Heinemann, 2017.